Journal of Sound and Vibration (2000) **237**(5), 819–836
doi:10.1006/jsvi.2000.3078, available online at http://www.idealibrary.com on IDEAL®

SPECTRAL-ELEMENT-BASED SOLUTIONS FOR WAVE PROPAGATION ANALYSIS OF MULTIPLY CONNECTED UNSYMMETRIC LAMINATED COMPOSITE BEAMS

D. Roy Mahapatra and S. Gopalakrishnan

Aerospace Engineering Department, Indian Institute of Science, Bangalore 560012, *India.*
E-mail: krishnan@aero.iisc.ernet.in

and

T. S. Sankar

Department of Automation and Production Engineering, École de Technologie Supérieure, University of Quebec, Montreal, Canada H3C 1K3

(*Received* 15 *May* 2000, *and in final form* 16 *May* 2000)

A spectrally formulated element that has three degrees of freedom (axial motion, transverse motion and rotation) per node for analysis of slender multiply connected composite beams under high-frequency impact loading is presented. The model represents a linear distributed parameter system. The element has an exact dynamic stiffness matrix as it is derived from exact solution to the governing wave equation in frequency domain. The present element can handle any kind of cross-sectional unsymmetry due to ply orientation. The results from the present formulation are compared with the results from a time domain finite element model based on linear axial and cubic transverse displacement field. It is shown that the formulated element is able to predict the reflected and transmitted response accurately through a rigid angle joint for varying joint angles and axial–flexural coupling. Also, the effect of ply-stacking sequence on dynamic response is illustrated. With this approach, a very large composite 2-D beam network can be analyzed under high-frequency impact loading with much smaller system size and lower computational cost compared to time domain finite element method.

© 2000 Academic Press

1. INTRODUCTION

The effect of impact on laminated composite structures is a crucial issue which researchers have tried to address with an increasing emphasis. The main reason is that the way these laminated fiber-reinforced structures are constructed, it contributes to high ratios of the longitudinal to the lateral elastic moduli, and in addition, it has significant layer-wise anisotropy due to ply orientations. One of the critical aspects is that the steep and discontinuous bending stress gradient at the ply interfaces may cause eventual delamination or debonding of the layers, thus putting the structural integrity in question. Starting from manufacturing, and throughout their design life, these structures are vulnerable to highly transient loading such as tool drop and other kinds of impact. These loading have very small duration (μs range). Hence, the energy of the system is confined over a large frequency band, exciting all the higher order modes. Other than the local damages, these disturbances generate stress waves that propagate through the structure. Also, an initial compressive

0022-460X/00/450819 + 18 $35.00/0 © 2000 Academic Press

pulse can develop tensile stresses due to the effects of local inhomogeneity [1]. The incident stress waves interact with the joints and boundaries and give rise to totally different types of wave. In addition, the responses become even more complicated if there is cross-sectional unsymmetry due to composite ply stacking which gives rise to axial–flexural coupling. Therefore, an efficient computational tool becomes necessary to study the effect of ply orientation on the dynamic response and the effect of exciting frequency range on the propagation of coupled axial–flexural waves. The proposed formulation is aimed towards this study.

The layer-wise construction of fiber-reinforced composite beam has a great advantage for embedding different class of functional materials such as piezoelectric ceramic, relaxor and anti-ferroelectric thin films, magnetostrictive plate strips and particle layers mixed with matrix [2–4]. Such configurations necessarily lead to cross-sectional unsymmetry. The axial–flexural coupling due to unsymmetric construction across the thickness of the beam or discontinuities in some layers, may give rise to additional progressive waves which are unlikely in a beam made up of homogeneous material. There are very few literature available which consider the axial–flexural coupling in the dynamics of laminated beams. Among these, the work done by Eisenberger *et al.* [5] presents a dynamic stiffness, formulated considering the displacement field as infinite and convergent recurring series. In most of the works on this issue reported so far (e.g., references 5–7]), mainly natural frequencies and mode shapes have been studied, and no data is available regarding the nature of perturbation in the actual response caused by axial–flexural coupling. Also, a similar effect on impact-induced wave propagation is yet to be addressed.

For laminated composite beams, it has been well established that shear deformation and rotary inertia play a key role in the prediction of responses. In this regard, Kant and Marur [8] have shown the effects of shear deformation introduced by higher order refined theory on the transient response of laminated composite beams. However, these effects are dependent on length-to-depth ratio (L/h) of the beam. As seen in the work of Chandrashekhara *et al.* [9], first order shear deformation theory (FSDT) including rotary inertia, and Euler–Bernoulli theory (EBT) produce identical results for a slender beam ($L/h > 100$). In addition, Bhimaraddi [10] has derived one perturbation solution which shows that the error in the first natural frequency predicted by EBT for cross-ply beam with $L/h > 20$ is well within 5% compared to that predicted by parabolic shear deformation (PSD) theory. The proposed spectral element is derived, based on EBT with rotary inertia neglected. Therefore, the analysis presented in this paper will be applicable to wave propagation in slender multiply connected beams and frames.

For an applied load that have very high-frequency content, the associated wavelengths become smaller at higher frequencies. In order to capture all the higher modes, the usual finite element model (FEM) requires very small element size to match the wavelength. This increases the system size enormously, and hence the conventional finite element method becomes prohibitive from computational aspect. In addition, this discretized model is exposed to crude error-bound approximation due to the numerical stability limit in computation. Another type of solution schemes which is suitable for the analysis of large-scale frames, is based on the concept of transfer function matrix and joint coupling matrix [11]. Further advancement in this direction is found in the work of Pao *et al.* [12], which incorporates the concept of scattering and reverberation matrices. Essentially, it can accommodate the effect of higher modes. But, generalization of such matrix methodology becomes very complicated when joints and discontinuities of different types exist in a structure. In this study, a model based on frequency domain finite element methodology is proposed. We call this model as spectral element model (SEM). Unlike conventional FEM, the model uses exact solution to the governing wave equation in the frequency domain as

interpolation function for element formulation. This process yields an exact dynamic stiffness matrix that characterizes the inertial distribution accurately. Therefore, only one element is required between any two successive structural discontinuities. As a result, each continuous member in a framed network behaves as a structural waveguide and the system size becomes many orders of magnitude smaller than the conventional FEM. SEM formulation uses the fast Fourier transform (FFT) algorithm to transform the distributed parameters from time domain to frequency domain and vice versa [13]. As a result, the transient dynamics in the system obtained by a PDE, becomes a set of ODEs with frequency as a parameter. These ODEs are easily amenable for solution compared to the original PDE. Using this approach, the analysis of longitudinal wave propagation in isotropic rod has been carried out by Doyle [14]. Also, a spectral element formulation to analyze the flexural wave propagation in isotropic beam can be found in reference [15]. In the present paper, a generalized 2-D beam element is derived which employs all the ingredients of the above two analysis and can be used for wave propagation analysis of both symmetric and unsymmetric laminated composite multiply connected beams. In frequency domain, the operations on nodal variables are carried out after spatial discretization in a similar way as in conventional (time domain) finite element method. Elaborate discussions on this method can be found in the work of Gopalakrishnan *et al.* [16] and Doyle and Farris [17]. One of the important aspects of the approach is that it enables the determination of not only the responses due to high-frequency loading, but also the associated phase change as the wave propagates from one location to another.

In the next section, we derive the mathematical model of the distributed parameter system. Next, the effects of axial–flexural coupling on phase and group dispersions are illustrated. The spectral element formulation is presented next, along with the computational scheme. In the numerical study, first the accuracy of the SEM results are validated by comparing with FEM results for a cantilever unsymmetric composite beam. Then the effect of axial–flexural coupling is demonstrated graphically. Finally, the nature of reflected and transmitted waves through a rigid angle joint are studied. Also, different ply-stacking sequences are considered to observe the effect of axial–flexural coupling on the response.

2. MATHEMATICAL MODEL

Considering Euler–Bernoulli theory for a general laminated composite thin beam, the axial and the transverse displacement field can be expressed as

$$U(x, y, z, t) = u^o(x, t) - zw(x, t)_{,x}, \quad W(x, y, z, t) = w(x, t), \tag{1}$$

where u^o is the axial displacement along the middle plane and w is the transverse displacement as shown in Figure 1(a). z is measured from the middle plane. The layer-wise constitutive law is defined as

$$\sigma_{xx} = \bar{Q}_{11}\varepsilon_{xx}, \tag{2}$$

where σ_{xx} and ε_{xx} are stress and strain in the x direction. The expression for $\bar{Q}_{11}$ can be found in reference [18]. The strain energy and the kinetic energy are defined as

$$S = \frac{1}{2}\int \sigma_{xx}\varepsilon_{xx}\,\mathrm{d}v, \qquad \Gamma = \frac{1}{2}\int \rho(\dot{u}^{o^2} + \dot{w}^2)\,\mathrm{d}v, \tag{3}$$

where $\dot{u}^o$ and $\dot{w}$ are the axial and transverse velocities, and ρ is the layer-wise density.

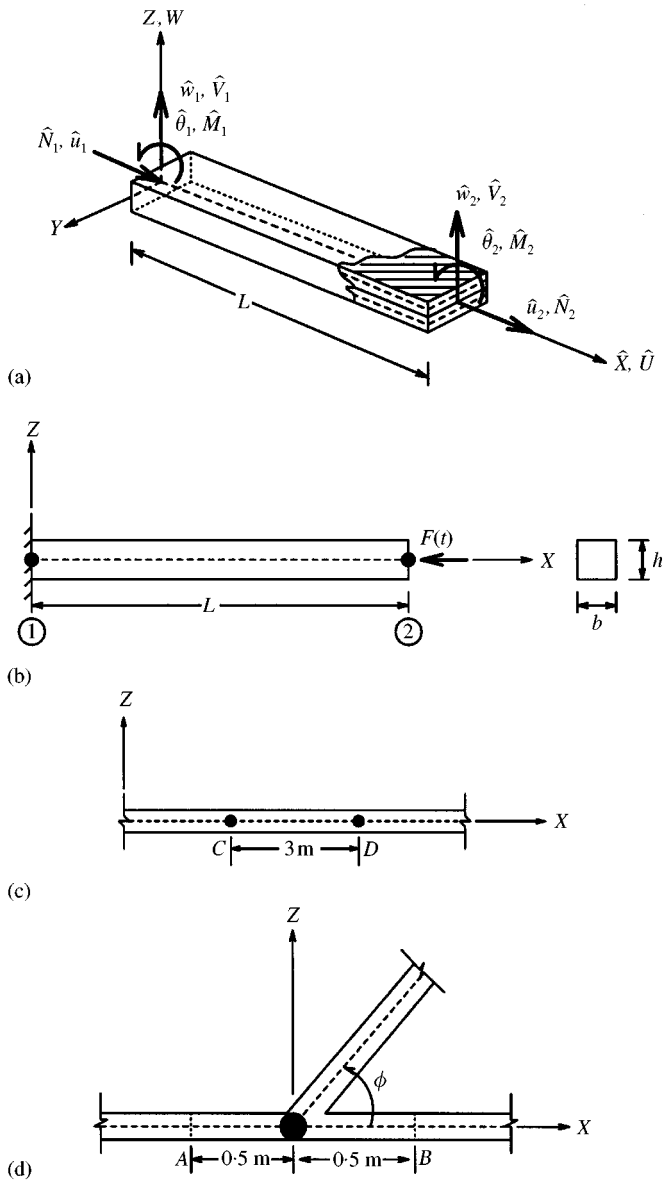

Figure 1. (a) Co-ordinate system and degrees of freedom for the spectral element; (b) AS/3501-6 graphite-epoxy $[0_5/90_5]$ composite cantilever beam with an impact load at the tip; (c) AS/3501-6 graphite-epoxy beam with infinite span; (d) Rigid angle joint with AS/3501-6 graphite-epoxy composite members.

Applying Hamilton's principle, the governing differential equations are obtained, and they can be expressed as

$$\rho A\ddot{u}^o - A_{11}u^o_{,xx} + B_{11}w_{,xxx} = 0, \qquad \rho A\ddot{w} - B_{11}u^o_{,xxx} + D_{11}w_{,xxxx} = 0 \tag{4, 5}$$

and the force boundary conditions are obtained as

$$A_{11}u^o_{,x} - B_{11}w_{,xx} = N_x, \qquad B_{11}u^o_{,xx} - D_{11}w_{,xxx} = V_x, \qquad -B_{11}u^o_{,x} + D_{11}w_{,xx} = M_x, \tag{6–8}$$

where

$$[A_{11}, B_{11}, D_{11}] = \int_{-h/2}^{+h/2} \bar{Q}_{11}\,[1, z, z^2]\,\mathrm{b}\,\mathrm{d}z, \tag{9}$$

h is the depth of the beam, b is the layer width and A is the cross-sectional area of the beam. $\ddot{u}^o$ and $\ddot{w}$ are the axial and transverse accelerations. $\langle\cdot\rangle_{,x}$, $\langle\cdot\rangle_{,xx}\ldots$ represent partial derivatives with respect to x. N_x is the axial force, V_x is the shear force and M_x is the bending moment. The governing differential equations (4) and (5) represent a system of coupled linear partial differential equations, which are difficult to solve exactly in the time domain for all boundary conditions. The spectral element method begins by transforming the field variables (displacements) on to the frequency domain using discrete Fourier transform (DFT). Thus, the discretized spectral form of the displacement field in terms of structural frequency (ω_n) is expressed as

$$u^o(x, t) = \sum_{n=1}^{N} \hat{u}(x, \omega_n)\mathrm{e}^{\mathrm{i}\omega_n t} = \sum_{n=1}^{N} (\tilde{u}_j \mathrm{e}^{-\mathrm{i}k_j x})\,\mathrm{e}^{\mathrm{i}\omega_n t}, \tag{10}$$

$$w(x, t) = \sum_{n=1}^{N} \hat{w}(x, \omega_n)\mathrm{e}^{\mathrm{i}\omega_n t} = \sum_{n=1}^{N} (\tilde{w}_j \mathrm{e}^{-\mathrm{i}k_j x})\,\mathrm{e}^{\mathrm{i}\omega_n t}, \tag{11}$$

where $\mathrm{i} = \sqrt{-1}$. $\hat{\langle\cdot\rangle}$ represents the frequency-dependent coefficients, and we call these as spectral amplitude of the transformed variables. $\tilde{u}_j$ and $\tilde{w}_j$ represent the wave coefficients, which are to be evaluated from three displacement and three force boundary conditions. k_j is the wavenumber associated with jth mode of propagation.

Subsituting equations (10) and (11) into governing differential equations (4) and (5), we get

$$\begin{bmatrix} (c_L^2 k_j^2 - \omega_n^2) & \mathrm{i}\dfrac{c_c^3}{\omega_n} k_j^3 \\ -\mathrm{i}\dfrac{c_c^3}{\omega_n} k_j^3 & \left(\dfrac{c_b^4}{\omega_n^2} k_j^4 - \omega_n^2\right) \end{bmatrix} \begin{Bmatrix} \tilde{u}_j \\ \tilde{w}_j \end{Bmatrix} = 0. \tag{12}$$

Here, c_L and c_b are the phase speeds of axial and flexural waves respectively. They are expresses as

$$c_L = \sqrt{\frac{A_{11}}{\rho A}}, \qquad c_b = \sqrt{\omega_n}\ \sqrt[4]{\frac{D_{11}}{\rho A}}. \tag{13}$$

The phase speed of the induced dispersive wave due to unsymmetric ply orientation causing axial–flexural coupling is defined as

$$c_c = \sqrt[3]{\omega_n \frac{B_{11}}{\rho A}}. \tag{14}$$

From equation (12), a sixth order characteristic equation is obtained, for the solution of wavenumber k_j, which is given by

$$(1 - r)k_j^6 - k_L^2 k_j^4 - k_b^4 k_j^2 + k_L^2 k_b^4 = 0, \tag{15}$$

where a non-dimensional axial–flexural coupling parameter is introduced as

$$r = \frac{B_{11}^2}{A_{11} D_{11}} \tag{16}$$

and the fundamental wavenumbers corresponding to uncoupled axial and flexural modes are defined, respectively, as

$$k_L = (\omega_n/c_L), \qquad k_b = (\omega_n/c_b). \tag{17}$$

Explicit expression for the six roots ($\pm k_1, \pm k_2, \pm k_3$) of equation (15) are given by

$$k_1 = \sqrt{\alpha}, \qquad k_2, k_3 = \frac{1}{\sqrt{2}} \sqrt{\left[\frac{k_L^2}{(1-r)} - \alpha\right] \pm \sqrt{\left[\frac{k_L^2}{(1-r)} + \alpha\right]^2 - 4\left[\alpha^2 - \frac{k_b^4}{(1-r)}\right]}},$$

where $\sqrt{\alpha}$ is the positive real root, evaluated numerically from equation (15). The spectral amplitudes of the displacement field is then explicitly redefined as

$$\begin{Bmatrix} \hat{u}(x, \omega_n) \\ \hat{w}(x, \omega_n) \end{Bmatrix} = \begin{bmatrix} R_{11} & R_{12} & R_{13} & R_{14} & R_{15} & R_{16} \\ R_{21} & R_{22} & R_{23} & R_{24} & R_{25} & R_{26} \end{bmatrix} \begin{Bmatrix} \tilde{u}_1 \, e^{-ik_1 x} \\ \tilde{u}_2 \, e^{-ik_1 (L-x)} \\ \tilde{w}_3 \, e^{-ik_2 x} \\ \tilde{w}_4 \, e^{-ik_2 (L-x)} \\ \tilde{w}_5 \, e^{-ik_3 x} \\ \tilde{w}_6 \, e^{-ik_3 (L-x)} \end{Bmatrix}, \tag{18}$$

where R_{1j} and R_{2j} are the amplitude ratios for the jth mode of propagation. These are derived from equation (12), and can be expressed as

$$R_{11} = 1 = R_{12}, \qquad R_{13} = -i\sqrt{r}\,\frac{k_L k_2^3}{k_b^2 (k_2^2 - k_L^2)} = -R_{14},$$

$$R_{15} = -i\sqrt{r}\,\frac{k_L k_3^3}{k_b^2 (k_3^3 - k_L^2)} = -R_{16}, \qquad R_{21} = i\sqrt{r}\,\frac{k_b^2 k_1^3}{k_L (k_1^3 - k_b^4)} = -R_{22},$$

$$R_{23} = 1 = R_{24}, \qquad R_{25} = 1 = R_{26}. \tag{19}$$

It is interesting to note that for a symmetric ply orientation, the axial–flexural coupling parameter r becomes zero. As a consequence, axial and flexural effects become uncoupled and equation (15) gives two equations. One is a second order characteristic equation, similar to that in case of elementary rod with roots $\pm k_L$ and the other is a fourth order characteristic equation, similar to that in case of a homogeneous Euler–Bernoulli beam with root $\pm k_b$ and $\pm ik_b$ as given in reference [13]. In this uncoupled case, R_{13}, R_{14}, R_{15}, R_{16}, R_{21} and R_{22} also become zero.

3. SPECTRUM AND DISPERSION RELATIONS

From design consideration, one big advantage of using laminated composite is that it can be tailored to get the required strength and stiffness by different ply orientations. The maximum axial–flexural coupling that one gets from such natural ply stacking (other than the inclusion of any other materials in the form of thin films, fibers or particle layers) is when

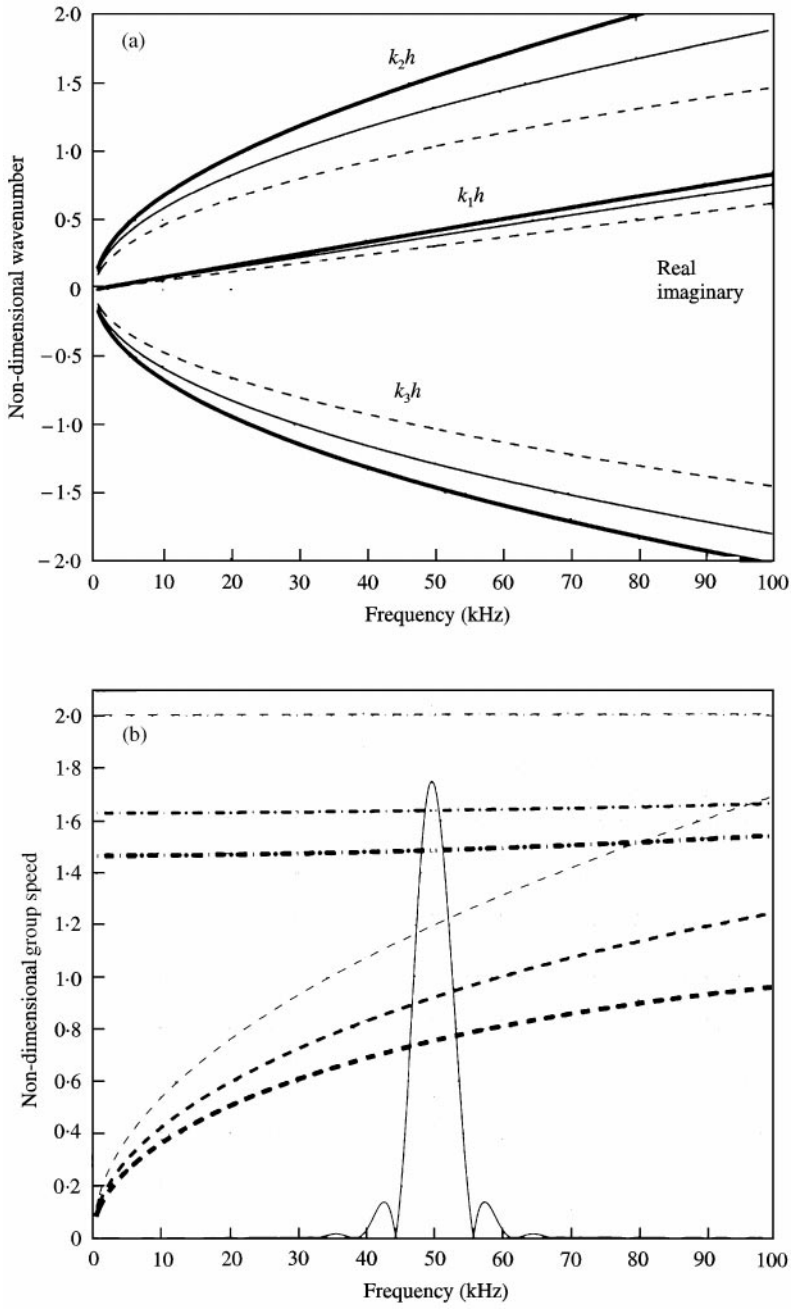

Figure 2. (a) Spectrum relation for various axial–flexural coupling; – – $r = 0{\cdot}0$; — $r = 0{\cdot}312$; —— $r = 0{\cdot}574$. (b) Dispersion relation for various axial–flexural coupling (—frequency amplitude of a modulated sinusoidal pulse): · – · – C_{g1}/C_0, $r = 0{\cdot}0$; · – – · C_{g1}/C_0, $r = 0{\cdot}312$; · – – · C_{g1}/C_0, $r = 0{\cdot}574$; – – – C_{g2}/C_0, $r = 0{\cdot}0$; – – C_{g2}/C_0, $r = 0{\cdot}312$; – – C_{g2}/C_0, $r = 0{\cdot}574$.

the cross-plies and 0° plies are stacked in separate groups. A generalization of the effect of axial–flexural coupling gives some valuable insights, when the spectrum relation (Figure 2(a)) and the dispersion relation (Figure 2(b)) are studied. AS/3501-6 graphite-epoxy plies (thickness of each layer is 1·0 mm) with three stacking sequences $[0_{10}]$ ($r = 0{\cdot}0$),

$[0_5/30_2/60_3]$ ($r = 0{\cdot}312$) and $[0_5/90_5]$ ($r = 0{\cdot}574$) are considered. In Figure 2(a), it can be observed that corresponding to axial mode (Mode 1) and flexural modes (Modes 2 and 3), the wavenumbers increase in magnitude for increasing coupling. However, this increase in Mode 2 (propagating component) is more than that in Mode 3 (evanescent component). Figure 2(b) also shows the variation of group speed $C_g = \mathrm{d}\omega/\mathrm{d}k_j$ normalized with the parameter $C_0 = \sqrt{E/\rho}$ (speed in aluminium). From these plots, it is clear that the axial speed is reduced by more than 26% due to the presence of unsymmetry arising from cross-ply stacking in groups. Also at a range of 50 kHz, the flexural speed of propagation is reduced by 42% for maximum coupling.

4. SPECTRAL ELEMENT FORMULATION

Two special cases arise in the dynamics of connected beams. One is finite length beam that is connected at both ends. The other is when the member extends to infinity. This will be referred to as a single noded or throw-off element. The behavior of both of these are fundamentally different and so will be treated separately. Since the elements will be derived in frequency domain, all the conventional nodal measures such as nodal displacement, strain, stress, force, etc. will correspond to their spectral amplitudes.

4.1. FINITE LENGTH ELEMENT

A two noded finite element of length L with nodal displacements and forces as shown in Figure 1(a) is considered. Using the explicit expression for displacement field given by equation (18), the nodal displacements $\hat{u}_1 = \hat{u}(0, \omega_n)$, $\hat{w}_1 = \hat{w}(0, \omega_n)$, $\hat{\theta}_1 = \hat{\theta}(0, \omega_n)$, $\hat{u}_2 = \hat{u}(L, \omega_n)$, $\hat{w}_2 = \hat{w}(L, \omega_n)$ and $\hat{\theta}_2 = \hat{\theta}(L, \omega_n)$ are expressed in terms of the wave coefficients $\tilde{u}_j$, $\tilde{w}_j$ as

$$\{\hat{u}\} = [\hat{T}]\{\tilde{u}\}, \tag{20}$$

where $\{\hat{u}\} = \{\hat{u}_1 \ \hat{w}_1 \ \hat{\theta}_1 \ \hat{u}_2 \ \hat{w}_2 \ \hat{\theta}_2\}^{\mathrm{T}}$ and $\{\tilde{u}\} = \{\tilde{u}_1 \ \tilde{u}_2 \ \tilde{w}_3 \ \tilde{w}_4 \ \tilde{w}_5 \ \tilde{w}_6\}^{\mathrm{T}}$. $[\hat{T}]$ is a 6×6 unsymmetric, non-singular matrix, which is a function of frequency, material properties and dimension of the element. This matrix represents the local wave characteristic of the displacements.

Next, using the expressions for force boundary condition from equations (6)–(8), the nodal forces are related to the wave coefficients $\tilde{u}_j$ and $\tilde{w}_j$ through the following force boundary equations:

$$\begin{aligned} &\hat{N}_1 = -\hat{N}_x(0, \omega_n), \qquad \hat{V}_1 = -\hat{V}_x(0, \omega_n), \qquad \hat{M}_1 = -\hat{M}_x(0, \omega_n), \\ &\hat{N}_1 = -\hat{N}_x(L, \omega_n), \qquad \hat{V}_1 = \hat{V}_x(L, \omega_n), \qquad \hat{M}_1 = \hat{M}_x(L, \omega_n). \end{aligned} \tag{21}$$

In matrix notation, this can be written as

$$\{\hat{F}\} = [\hat{P}]\{\tilde{u}\}, \tag{22}$$

where the force vector $\{\hat{F}\} = \{\hat{N}_1 \ \hat{V}_1 \ \hat{M}_1 \ \hat{N}_2 \ \hat{V}_2 \ \hat{M}_2\}^{\mathrm{T}}$. The matrix $[\hat{P}]$ has properties that are similar to $[\hat{T}]$, and it represents the local wave characteristic of forces. Combining

equations (20) and (22), the equilibrium equation is obtained as

$$\{\hat{F}\} = [\hat{P}]\,[\hat{T}]^{-1}\,\{\hat{u}\} = [\hat{K}]\,\{\hat{u}\}, \tag{23}$$

where $[\hat{K}]$ is the symmetric dynamic stiffness matrix for an unsymmetric composite beam element as a complex function of frequency.

4.2. THROW-OFF ELEMENT

Unlike conventional finite element, here we derive a special case when the beam is very long, and application of any transient load at any location causes no secondary disturbances other than incident waves departing that location. This simulates a condition, wherein the boundaries are at such a distance that the effect of reflected waves become negligible due to attenuation throughout their long traversal, and do not reach the location under consideration within the time of observation. In other words, throw-off element is a non-resonant single-node element that acts as a conduit to allow the propagation of trapped energy out of the system. Considering only the incident part of the displacement field given by equation (18), the field variables for throw-off element can be written as

$$\begin{Bmatrix} \hat{u}(x, \omega_n) \\ \hat{w}(x, \omega_n) \end{Bmatrix} = \begin{bmatrix} R_{11} & R_{13} & R_{15} \\ R_{21} & R_{23} & R_{25} \end{bmatrix} \begin{Bmatrix} \tilde{u}_1 \, e^{-ik_1 x} \\ \tilde{w}_3 \, e^{-ik_2 x} \\ \tilde{w}_5 \, e^{-ik_3 x} \end{Bmatrix}. \tag{24}$$

Using the same procedure as followed in the case of finite length element formulation in previous subsection, a 3×3 symmetric dynamic stiffness matrix $[\hat{K}]$ as a complex function of frequency is derived.

4.3. COMPUTER IMPLEMENTATION

Before performing the analysis, the given time-dependent input force is transformed into a series of frequency components using forward FFT. These are read in along with the complex amplitudes of the force. The program architecture is almost identical to that of conventional finite element program in terms of input, assemblage, system solving and output. The major difference is that the assemblage is done as part of a loop over all the members at each frequency. For each member, the local dynamic stiffness is established and then transformed to global co-ordinates. Then it is entered into the structural stiffness matrix, simply by associating the appropriate nodal numbers. Those nodes which have a zero d.o.f. are not entered at all. The non-zero nodal d.o.f. of the resulting system are obtained using a banded solver.

Rather than solving a specific loading history, the system is first solved for a unit impulse by inverting the global dynamic stiffness matrix at each frequency. This yields the system transfer function at the nodes, which are stored for later use. The transfer function enables one to obtain the response to any excitation from a simple convolution. Thus, the problem can be thought of as a sequence of pseudo-static problem for each of N frequencies. Note that the number of d.o.f. is usually quite small, because the nodes are situated at joints. Therefore, unlike conventional finite element method, the process of inverting and storing transfer functions are not prohibitive from the computational view-point.

Because the spectral elements span long distances, it is usually necessary to determine the responses at intermediate locations. This is done by first evaluating the frequency-dependent coefficients in the kernel solution to obtain the member responses at desired location. As the final step, time reconstructions are obtained by inverse FFT.

5. RESULTS AND DISCUSSION

5.1. CANTILEVER BEAM

In order to study the quality of the response obtained from the proposed frequency domain SEM, the results are first compared with results obtained from time domain FEM. For this purpose, a finite element model is employed where the elements has the following mid-plane displacement field.

$$u^o(x, t) = C_1 + C_2 x \qquad w(x, t) = C_3 + C_4 x + C_5 x^2 + C_6 x^3. \tag{25}$$

A cantilever beam as shown in Figure 1(b) is considered with length $L = 1{\cdot}0$ m, width $b = 0{\cdot}01$ m, depth $h = 0{\cdot}01$ m, and made up of AS/3501-6 graphite-epoxy, having properties $E_1 = 144{\cdot}48$ GPa, $E_2 = 9{\cdot}632$ GPa, $G_{12} = 4{\cdot}128$ GPa, $v_{12} = 0{\cdot}3$, $\rho = 1389$ kg/m^3. The ply-stacking sequence used is $[0_5/90_5]$, which gives a coupling factor $r = 0{\cdot}574$. An impact load of 4.4 N and 50 μs duration shown in Figure 3 is considered. The figure shows that the load has a very high-frequency content of about 50 kHz. This impact load is first applied at the cantilever tip in axial direction. In SEM, the whole beam is considered as a single element, whereas in FEM, the domain is modelled with 1000 elements (overall system size 3000×6). The Newmark time integration scheme with a time step of 1 μs is adopted. Figure 4(a) shows the comparison of axial tip velocities obtained from SEM and FEM.

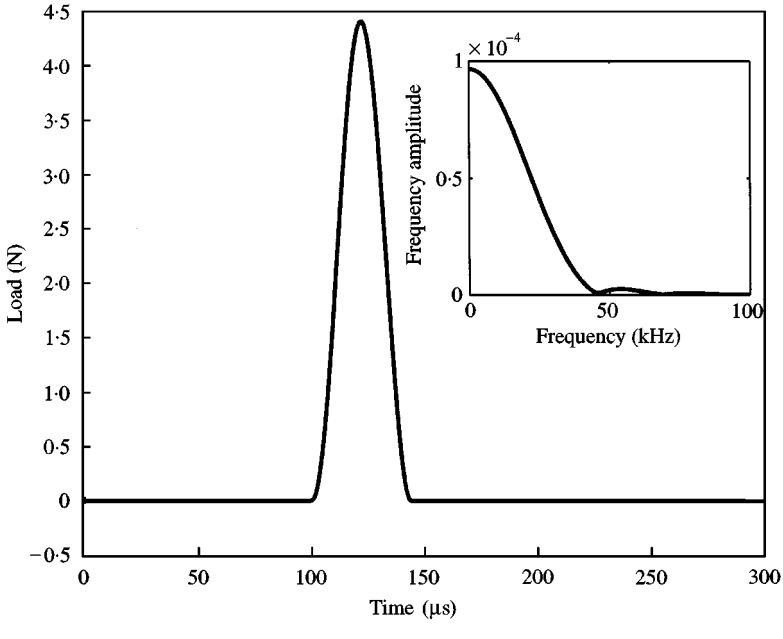

Figure 3. Impact load history. Frequency spectrum of the load is shown in the inset.

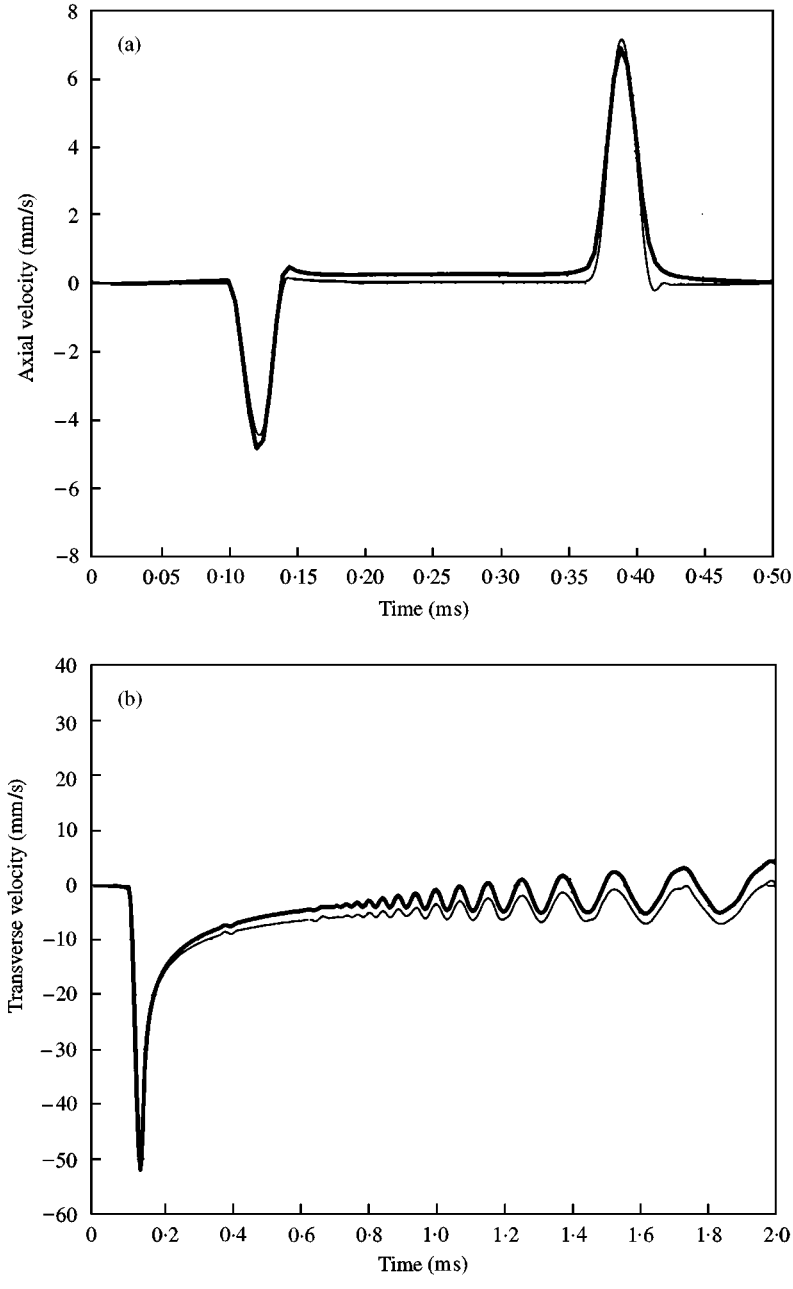

Figure 4. (a) Axial response at the cantilever tip due to axial tip load: ——— SEM; —— FEM. (b) Transverse response at the cantilever tip due to transverse tip load: ——— SEM; —— FEM.

Next, the beam is impacted in transverse direction at the tip and Figure 4(b) shows the comparison of transverse tip velocities. For both the cases, the plots show good agreement. From figure 4(a), it is clear that the axial wave propagates non-dispersively, while the flexural wave (shown in Figure 4(b)) is dispersive. Figure 4(b) also shows that the response

obtained by SEM is slightly on the higher side. This may be attributed to the different damping schemes employed by SEM and FEM.

5.2. EFFECT OF AXIAL–FLEXURAL COUPLING

One of the characteristics of the unsymmetric composite beam is the presence of axial-flexural coupling. That is, an incident axial wave will give rise to flexural wave and *vice versa*. The aim of the following example is to capture this behavior. In order to see this, it is required that the waves travel non-dispersively. Hence, for this purpose, a sinusoidally modulated pulse is allowed to propagate through an infinite beam shown in Figure 1(c). The pulse is modulated at 50 kHz frequency. The frequency amplitude of this pulse has been plotted with firm line in Figure 2(b). The infinite beam is modelled using two throw-off elements and one finite length element. Three ply-stacking sequences having coupling parameter $r = 0{\cdot}0$, $0{\cdot}312$ and $0{\cdot}574$ (as used in section 3) are considered. The modulated pulse is first applied in the axial direction at C. The axial and transverse velocity histories obtained at D, which is 3·0 m away from the application of load are shown in Figures 5(a) and 5(b) respectively. In Figure 5(a), the time shifts in the predominant axial mode response for increasing values of r can be attributed to the reduction in axial group speed (Mode 1 in Figure 2(b)). Also, for $r = 0{\cdot}574$, the effect of flexural mode induced in the axial response is clearly visible around 1·0 msec. The time of occurrence of this additional mode corresponds to the flexural group speed (Mode 2) in Figure 2(b) at 50 kHz, which happens to be the modulation frequency of the applied load. Similarly, in Figure 5(b), the increasing effect of both the modes induced in the flexural response is visible for increasing values of r, and their times of occurrence resemble those in Figure 5(a). Next, the same modulated pulse as considered above, is applied in transverse direction on the infinite beam at C. The tranverse and axial velocity histories at D are plotted in Figures 5(c) and 5(d) respectively. In Figure 5(c), it can be observed that the effect of the axial mode induced in the transverse response is of negligible order. Here, the time shifts in the flexural mode response for increasing values of r are greater than that in the axial mode response due to axial loading as shown in Figure 5(a), which correlate the fact that for the chosen modulation frequency (50 kHz), the percentage reduction of flexural group speed (Mode 2) is nearly 10% more than that of axial group speed as revealed from Figure 2(b). From Figure 5(d), for maximum value of coupling, two propagating pulses can be seen clearly—the first is due to axial mode and the second is due to the flexural mode. It is seen that the magnitude of the flexural mode is slightly higher compared to that of the axial mode. A general trend observed from the example is that there is increase in magnitude of the responses for increasing values of r, and this is attributed to the reduction in the strength of the structure with more off-axis ply orientations. Hence, by using SEM, the presence of two simultaneously propagating spectrum due to unsymmetric ply orientations becomes tractable in both quantitative as well as in qualitative forms.

5.3. ANGLE JOINT

Often in practice, we come across planar frame structures with complex geometry. Such structures are often used for space application such as solar panel, antenna, etc., wherein a number of skeletal members are connected by rigid or flexible joints, thereby creating a complex structural network. The proposed SEM can account for such situation with relative ease. In this paper, we consider a rigid angle joint with three composite members

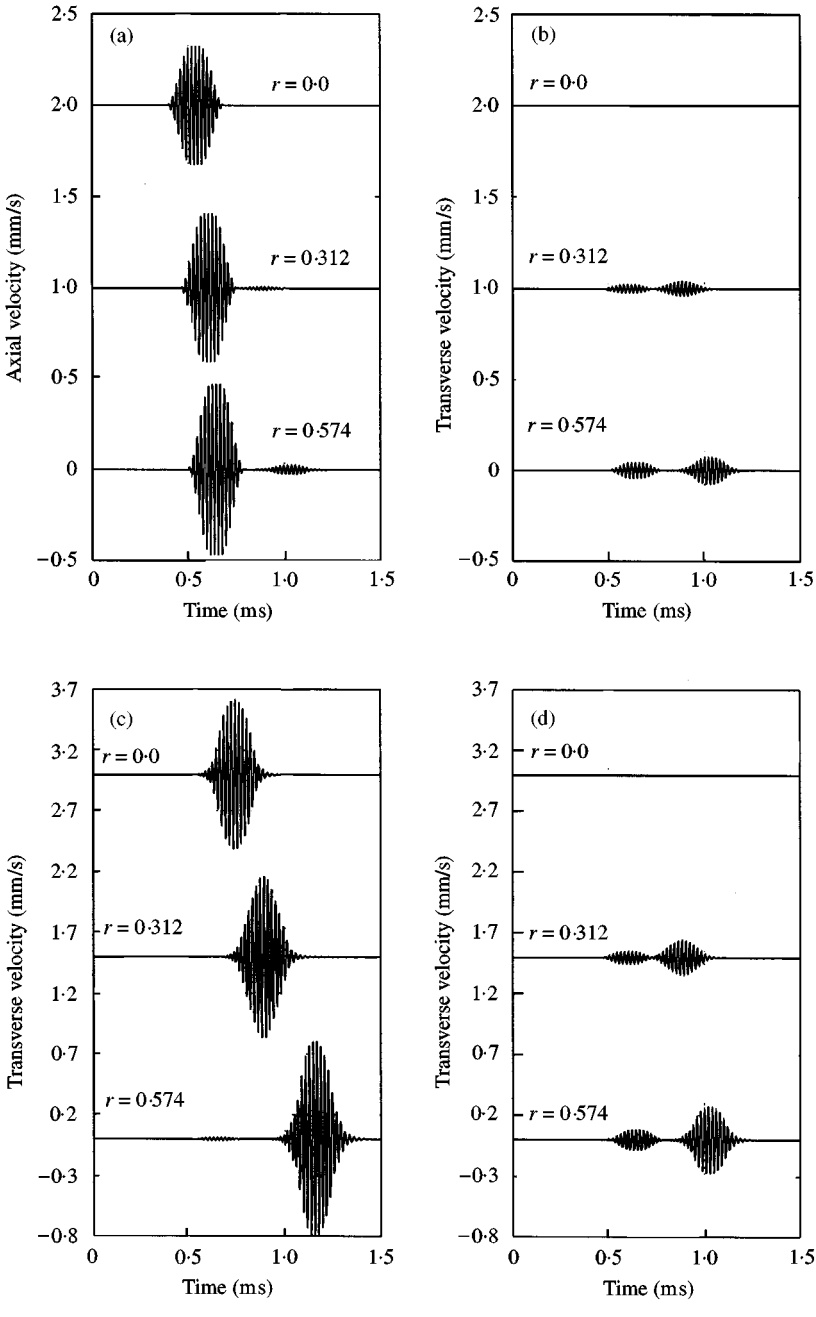

Figure 5. (a) Axial response and (b) Transverse response at D due to axial modulated pulse applied on the infinite beam at C. (c) Tranverse response and (d) axial response at D due to transverse modulated pulse applied on the infinite beam at C.

(Figure 1(d)) to analyze the nature of reflected and transmitted waves through the joint. In particular, it will be interesting to observe how the dynamics of the system changes with the change in joint angle. In addition, it is also important to know the effect of axial–flexural coupling on the overall response. In SEM, 0·5 m long segments on both sides of the joint

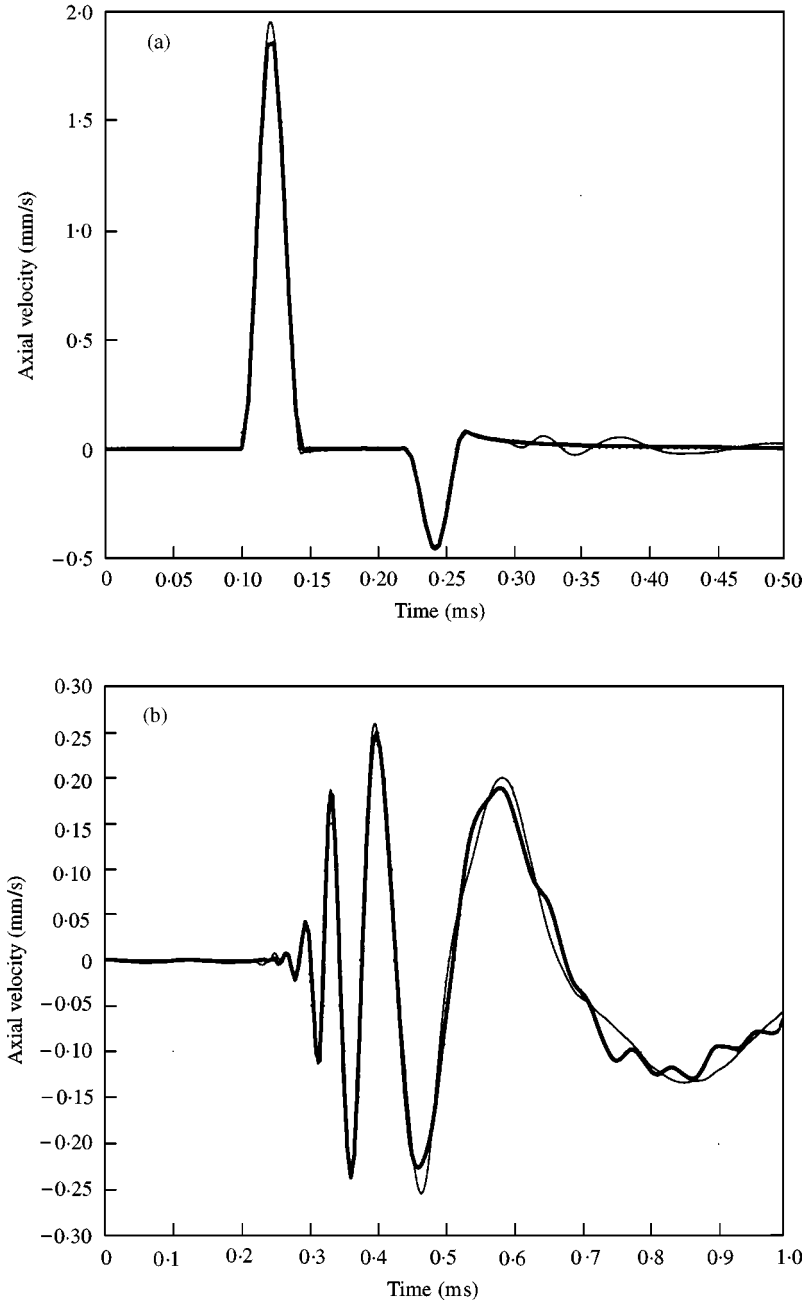

Figure 6. (a) Comparison of axial response at A, due to axial impact load applied at A. —— SEM; — FEM. (b) Comparison of axial response at A, due to transverse impact load applied at A. —— SEM; — FEM.

along the x-axis are modelled with two finite length spectral elements. Rest of the semi-infinite segments are modelled with three throw-off elements. In FEM, these three semi-infinite segments are modelled with 950 elements each, while the segment AB is modelled with 100 elements. The length of each element is 1·0 cm. This gives an overall system size of 8994×9.

Each member connected with the joint is made up of AS/3501-6 graphite-epoxy, as considered in the previous cases, and with ply-stacking sequence $[0_5/45_5]$. Here, the coupling factor $r = 0{\cdot}213$. First of all, to validate the accuracy of the response obtained from SEM, the impact load as considered earlier (Figure 3) is applied axially at A for joint angle $\phi = 30^\circ$. The axial velocity history at the same point A, is computed and compared with the FEM result, which is shown in Figure 6(a). Similarly, the same load is applied transversely at A. The axial velocity history at the same point A is computed, and also compared with the FEM result, which is shown in Figure 6(b). In the above two cases, both the results show good agreement.

Next, the effect of variation of joint angle ϕ, on transmitted response through the rigid joint (Figure 1(d)) is simulated. $[0_5/45_5]$ ply-stacking sequence ($r = 0{\cdot}213$) is considered in all the three members. The same axial loading (Figure 3) as considered earlier is applied at A. The transverse response at B is computed for various angles over the range 10–150°. Figure 8 shows the surface plot of the transverse velocity history normalized with $P_{max}c_L h^2/D_{11}$. Here, P_{max} is the maximum load ordinate (Figure 3). As seen in the spectrum plot (Figure 2(a)), the axial–flexural coupling has much lesser effect on axial wave number compared to that on flexural wave numbers. And this fact causes very little contribution of Mode 1 on transverse response compared to the contribution of Mode 2 on axial response, as observed in Figures 5(a) and 5(c). This is also clear from Figure 7, wherein the contribution of axial mode is so small that it is not visible. Figure 7 also shows that at small joint angles, and near $\phi = 90^\circ$, the peaks get reduced. Actually, this happens due to less amount of shear force transfer into the member containing the point B. In the other ranges fo ϕ, the magnitudes of the peaks become almost unchanged. Even though, the occurrence of these peaks get slightly shifted behind, for increasing values of ϕ.

To study the effect of axial–flexural coupling on the dynamic response, the same rigid joint (Figure 1(d)) with an axial loading at point A, is considered as in the previous case. The angle of the rigid joint ϕ is taken as 45°. The non-dimensional coupling parameter r is varied by using different ply-stacking sequences. Three-ply-stacking sequences $[0_{10}]$,

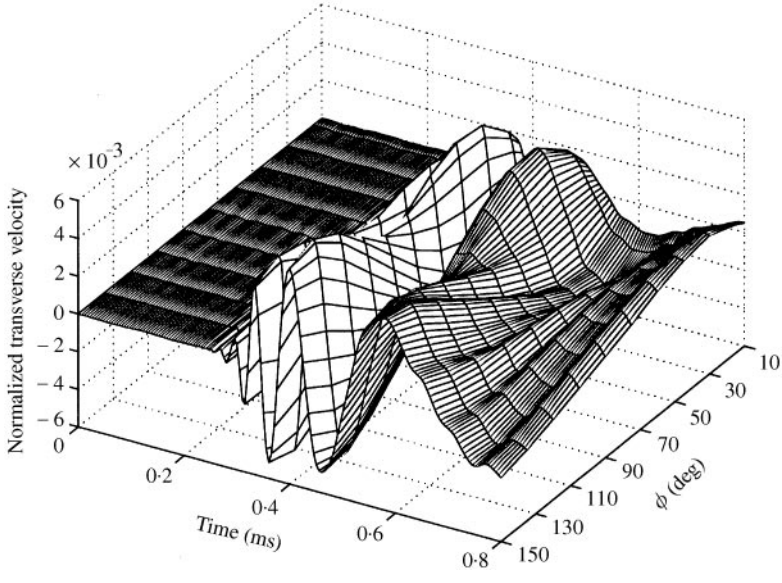

Figure 7. Transmitted transverse response at B, due to axial impact load applied at A, for various joint angles ϕ.

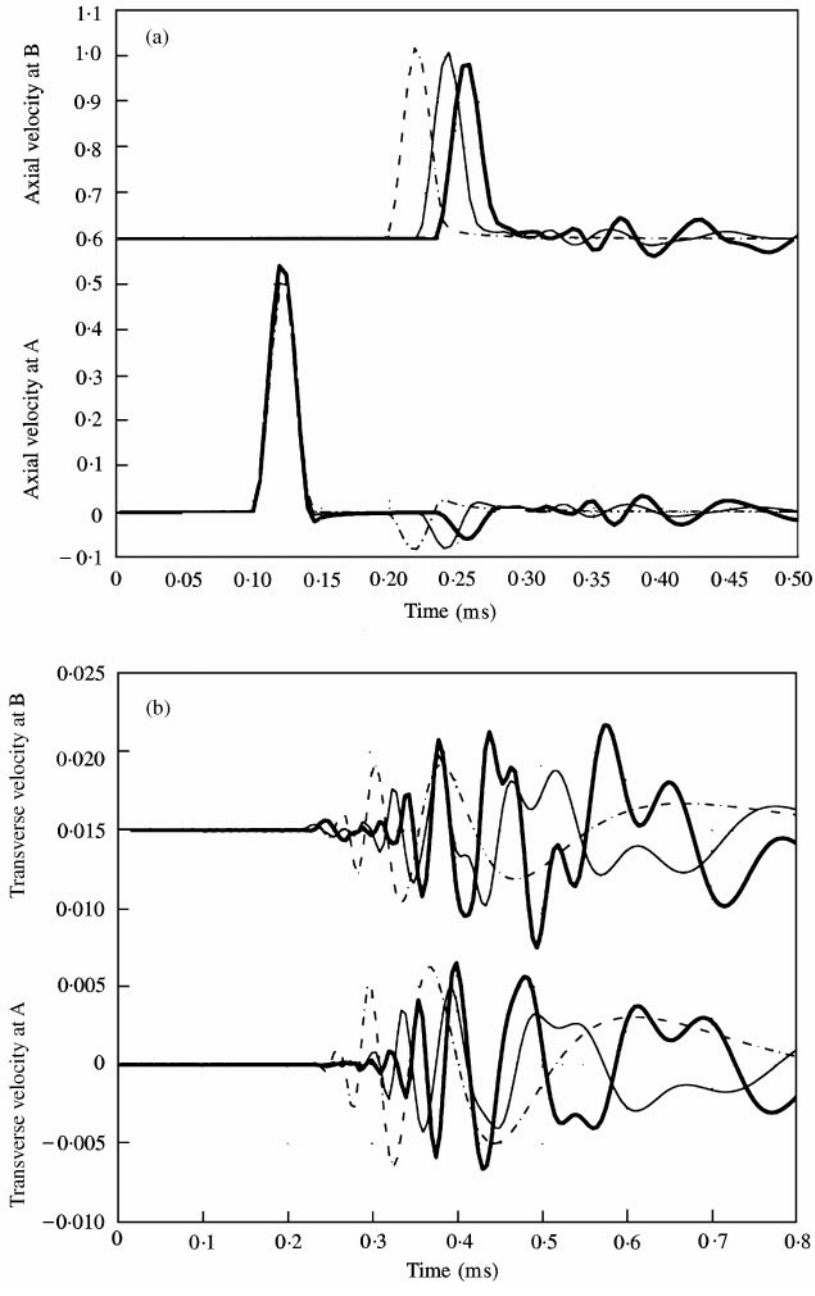

Figure 8. (a) Normalized axial velocity history at A and B, showing the reflection and transmission of response through the rigid joint ($\phi = 45°$), due to axial impact load applied at A: $\cdot - \cdot -$ $r = 0{\cdot}0$; —— $r = 0{\cdot}312$; ——— $r = 0{\cdot}574$. (b) Normalized transverse velocity history at A and B, showing the reflection and transmission of response through the rigid joint ($\phi = 45°$), due to axial impact load applied at A: $\cdot - \cdot -$ $r = 0{\cdot}0$; —— $r = 0{\cdot}312$; ——— $r = 0{\cdot}574$.

$[0_5/30_2/60_3]$ and $[0_5/90_5]$ are chosen, which produce coupling parameters $r = 0{\cdot}0$, $0{\cdot}312$ and $0{\cdot}574$ respectively. In Figure 8(a), the axial velocity (normalized with $P_{max}c_L/A_{11}$) response at A and B (both are at a same distance of 0·5 m from the joint) is plotted. The figure shows that the reflected axial response at A, as well as the transmitted axial response

at B reaches at the same time for a particular value of r. But, due to the decrease in the values of A_{11}, for increasing values of r, the axial speed of propagation decreases. As a result, both the responses reach at a later stage. A separation of 0·24 m can be seen between responses due to unsymmetric cross-ply and the symmetric 0° ply configurations. Also, an increasing nature of dispersiveness becomes dominant after the initial peak, which can be considered as a contribution from Modes 2 and 3, as discussed earlier. Figure 8(b) shows the plot of transverse velocity (normalized with $P_{max}c_L h^2/D_{11}$) response at A and B. Other than a similar time lag in the arrival of reflected and transmitted responses as observed in the case of axial propagation, the smoothness in the response curves disappears and transient nature becomes significant for increasing values of r. The local kinks at the later stages necessarily appear as a very-high-frequency contribution from Mode 1 propagation.

6. CONCLUSIONS

A methodology, analogous to that of finite element method, is presented that allow problems involving many connected elementary unsymmetric laminated composite waveguides to be handled in a convenient and straightforward manner.

Unlike conventional FE formulation, however, the length of the spectral element is not a limiting factor; each element is formulated exactly, irrespective of its length. Hence, structural connections and discontinuities are the factors which govern the length of the element. This leads to a substantial reduction in the number of equations that are to be solved. The work presented in this paper has mainly dealt with the behavior of elementary unsymmetric composite beams, without the effects of shear deformation and rotary inertia. Due to this reason, the numerical investigation has been restricted to slender beams and frames with unsymmetry. This is basically to avoid any appreciable deviation from the actual structural response.

It is seen from the numerical investigation that the main effect of unsymmetric ply orientation is the alteration of the spectrum and dispersion relations. It is found that the axial mode (Mode 1) is least affected by unsymmetry. However, the flexural modes (Modes 2 and 3) are most affected. That is, the flexural speeds are greatly reduced (about 20%) due to unsymmetry. The numerical studies have also shown that the results from the formulated spectral element agrees well with established finite element method. This study, through SEM, has clearly brought out the changes that an unsymmetric ply configuration can introduce to alter the dynamics of multiply connected symmetric composite beams.

Another big advantage of SEM is that the solution has very little storage requirement as compared to conventional FEM. In the actual computation of the third example (angle joint), it has been found that the storage requirement for system formation is approximately 2·05 KB for SEM in contrast to 1·5 MB for FEM. In SEM, 8-byte memory was assigned for handling each of the real and complex part of the stiffness elements in banded form, and in FEM, the same was assigned for handling the real-valued stiffness elements in banded form.

REFERENCES

1. F. C. Moon 1973 A critical survey of wave propagation and impact in composite materials. *NASA-CR*-121226. *Princeton University, U.S.A.*
2. D. Roy Mahapatra and S. Gopalakrishnan 1999 *Conference Proceedings of ISSS-SPIE on Smart Materials, Structures and Systems. Bangalore, India*, 337–342. Spectrally formulated finite element for elementary composite beam with embedded smart layers.

3. A. V. KRISHNAMURTY, M. ANJANAPPA and Y.-F. WU 1997 *Journal of Sound and Vibration* **206**, 133–149. The use of magnetostrictive particle actuators for vibration attenuation of flexible beams.
4. A. A. BENT 1997 *Ph.D. Thesis, Massachusetts Institute of Technology, U.S.A.* Active fiber composites for structural actuation.
5. M. EISENBERGER, H. ABRAMOVICH and O. SHULEPOV 1995 *Composite Structures* **31**, 265–271. Dynamic stiffness analysis of laminated beams using a first order shear deformation theory.
6. H. ABRAMOVICH and A. LIVSHITS 1994 *Journal of Sound and Vibration* **176**, 597–612. Free vibration of non-symmetric cross-ply laminated composite beams.
7. H. ABRAMOVICH, M. EISENBERGER and O. SHULEPOV 1996 *AIAA Journal* **34**, 1064–1069. Vibration and buckling of cross-ply nonsymmetric laminated composite beams.
8. S. R. MARUR and T. KANT 1988 *Composite Structures* **41**, 1–11. Transient dynamics of laminated beams: an evaluation with a higher-order refined theory.
9. K. CHANDRASHEKHARA, K. KRISHNAMURTHY and S. ROY 1990 *Composite Structures* **14**, 269–279. Free vibration of composite beams including rotary inertia and shear deformation.
10. A. BHIMARADDI 1994 *Composite Structures* **29**, 415–420. Computation of ply thickness of laminated beam for which Euler–Bernoulli theory is adequate.
11. R. J. NAGEM and J. H. WILLIAMS 1989 *Mechanical Structure and Machine* **17**, 349–371. Dynamic analysis of large space structure using transfer function matrices and joint coupling matrices.
12. YIH-HSING PAO, DER-CHING KEH and SAMUEL M. HOWARD 1999. American Institute of Aeronautics and Astronautics Journal **37**, 594–603. Dynamic response and wave propagation in plane trusses and frames.
13. J. F. DOYLE 1989 *Wave Propagation in Structures.* New York: Springer-Verlag.
14. J. F. DOYLE 1988 *International Journal of Analytical and Experimental Modal Analysis* **3**, 1–5. A spectrally formulated finite element for longitudinal wave propagation.
15. J. F. DOYLE and T. N. FARRIS 1990 *International Journal of Analytical and Experimental Modal Analysis* **5**, 13–23. A spectrally formulated finite element for flexural wave propagation in beams.
16. S. GOPALAKRISHNAN, M. MARTIN and J. F. DOYLE 1992 *Journal of Sound and Vibration* **158**, 11–24. A matrix methodology for spectral analysis of wave propagation in multiple connected timoshenko beam.
17. J. F. DOYLE and T. N. FARRIS 1990 *International Journal of Analytical and Experimental Modal Analysis* **5**, 223–237. A spectrally formulated finite element for wave propagation in 3-D frame structures.
18. J. N. REDDY 1997 *Mechanics of Laminated Composite Plates.* U.S.A. CRC Press.